Coarse-Grained Molecular Dynamics Simulations for Understanding the Impact of Short-Range Anisotropic Attractions on Structure and Viscosity of Concentrated Monoclonal Antibody Solutions

Amjad Chowdhury, Jonathan A. Bollinger, Barton J. Dear, Jason K. Cheung, Keith P. Johnston,* and Thomas M. Truskett*

Cite This: *Mol. Pharmaceutics* 2020, 17, 1748−1756

Read Online

ACCESS | Metrics & More | Article Recommendations | SI Supporting Information

ABSTRACT: Understanding protein−protein interactions in concentrated therapeutic monoclonal antibody (mAb) solutions is desirable for improved drug discovery, processing, and administration. Here, we deduce both the net protein charge and the magnitude and geometry of short-ranged, anisotropic attractions of a mAb across multiple concentrations and cosolute conditions by comparing structure factors $S(q)$ obtained from small-angle X-ray scattering experiments with those from molecular dynamics (MD) simulations. The simulations, which utilize coarse-grained 12-bead models exhibiting a uniform van der Waals attraction, uniform electrostatic repulsion, and short-range attractions between specific beads, are versatile enough to fit $S(q)$ of a wide range of protein concentrations and ionic strength with the same charge on each bead and a single anisotropic short-range attraction strength. Cluster size distributions (CSDs) obtained from best fit

simulations reveal that the experimental structure is consistent with small reversible oligomers in even low viscosity systems and help quantify the impact of these clusters on viscosity. The ability to systematically use experimental $S(q)$ data together with MD simulations to discriminate between different possible protein−protein interactions, as well as to predict viscosities from protein CSDs, is beneficial for designing mAbs and developing formulation strategies that avoid high viscosities and aggregation at high concentration.

KEYWORDS: antibody, high concentration, protein−protein interactions, small-angle X-ray scattering, structure factor, coarse-grained modeling, molecular dynamics simulations, self-association, viscosity
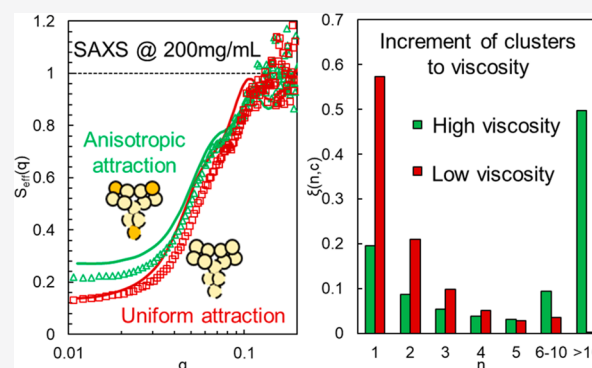
INTRODUCTION

Monoclonal antibodies (mAbs) are a promising class of therapeutics[1] whose utility for subcutaneous delivery can be hindered by a limited understanding of their interactions in solution at high concentrations. Due to interparticle distances at high concentration of only ∼1 nm,[2] local anisotropic (i.e., charge−charge, charge-dipole, dipole−dipole, hydrogen bonding, and hydrophobic) protein−protein interactions (PPIs) may promote the formation of reversible oligomers, which can lead to viscosities above the practical threshold of ∼20 cP for subcutaneous delivery.[2−5] Therefore, characterizing the effects of PPI on structure and rheology as a function of protein concentration, along with solution conditions including pH, ionic strength, and the concentration of excipients including cosolutes, is of great interest in improving mAb discovery and formulation relevant to processing, storage, and delivery.[6,7]

The influence of PPI on the structure of protein solutions at high concentration may be interrogated at length scales from ∼1 nm to ∼100 nm with small-angle X-ray or neutron scattering (SAXS/SANS).[21−25] These techniques can be used to directly probe the complex multibody effective interactions between mAbs prevalent at high concentration. In contrast, only two-body interactions can be characterized via diffusion interaction parameters (k_D) and/or the second virial coefficients (B_{22}), typically at concentrations below 20 mg/mL.[8−13] Furthermore, SAXS/SANS yields a structure factor $S(q)$ over a wide range of scattering wavenumber $q = (4\pi/\lambda)\sin(\theta/2)$ from ∼0.01 Å^{-1} to ∼0.1 Å^{-1},[14] where θ is the scattering angle and λ is the wavelength. The ability to study structure at multiple length scales allows for the analysis of mAb conformations and spatial correlations at much finer

dimensions[15,16] than with static light scattering (SLS) measurements with $q \sim 0.001$ A^{-1}.[17−21]

The effect of mAb shape and local anisotropic interactions on PPI may be inferred from MD simulations of experimental $S(q)$ data with 12-bead coarse-grained (CG) models. These models have been used to simulate the formation of reversible oligomers at high concentration, which have a marked effect on colloidal stability and viscosities of mAb solutions.[22−24] Although SLS $S(0)$ behavior of mAb solutions at high concentration may be predicted from 12-bead model parameters fit with low concentration B_{22} data, deviations grow as interprotein spacing decreases with concentration.[25,26] Recently, a 12-bead model was also used to model SANS data across multiple concentrations to predict cluster sizes and to relate structure to mAb viscosity and diffusivity.[14,27] In many of these studies, anisotropy in the distribution of interactions on the protein surface arose only from the theoretical charges on each bead, which were calculated from the mAb sequence. However, due to effects of local changes in pK_a and counterion binding on the effective charge,[28−30,37] the inclusion of additional empirical fitting parameters in the model is often needed.[25] Furthermore, local, short ranged (e.g., hydrogen bonding, dipole−dipole, or hydrophobic) interactions cannot be readily predicted from electrostatic Coulombic potentials alone. As an alternative, we inferred local short-ranged attractions on specific beads from 12 bead model simulations of experimental SAXS scattering data.[31,32] However, these models did not consider the effect of electrostatic repulsion and were therefore limited to high ionic strength systems where the effect of protein charge was highly screened. Thus, a key challenge would be to discover ways to balance the various interactions in CG models of experimental SAXS data to guide the understanding and correlation of bead-specific attraction to better understand their effect on protein structure.

Here, we perform new molecular dynamics (MD) simulations to reanalyze our recent SAXS results[31] with 12-bead CG models to capture the effects of bead-specific anisotropic short-range attraction in combination with a uniform background van der Waals (vdW) attraction and electrostatic repulsion on each bead. We hypothesize that the addition of both of these background terms to our earlier model, which only included bead-specific anisotropic short-range attraction, will lead to substantial improvement over a wide range of concentration and solution conditions. The effect of ionic strength is investigated by varying the concentration of the nonbinding cosolute NaCl. The PPIs are further tuned with binding cosolutes arginine or ZnSO$_4$. On the basis of comparisons to $S(q)$ at high ionic strength with attraction on selected beads (Fab−Fab only vs Fab−Fab, Fab−Fc, and Fc−Fc interactions), we gain molecular insights into the key effects of short-range anisotropic interactions. Furthermore, by fitting $S(q)$ at multiple ionic strengths, we extract the strength of net electrostatic repulsion and therefore an effective net protein charge. Upon considering the effect of electrostatic repulsion, our model accurately describes $S(q)$ behavior from 125 to 250 mg/mL protein concentration and 20−270 mM ionic strength using only a single attraction strength and net charge. Given $S(q)$, the simulations provide real-space properties including center-of-mass radial distribution functions $g_{COM}(r)$ and cluster size distributions (CSD) that are useful for understanding protein colloidal stability and viscosity. The CSDs are input into the Kastelic viscosity

model[33] to quantify the significant impact of small oligomeric clusters on the solution viscosity at high concentrations.

■ EXPERIMENTAL SECTION

MD simulations of improved 12-bead coarse-grained models are used to gain insight into how both short-range attractive interactions and electrostatic repulsion impact previously measured[31] $S(q)$ and shear viscosity of concentrated solutions of a mAb (mAb2). Every sample was formulated in 30 mM sodium acetate buffer at pH 5.5. The cosolutes arginine (Arg), NaCl, and zinc sulfate (ZnSO$_4$) were used to modulate the interactions and in some cases to lower the viscosity. As reported previously,[31] the relative positions of the beads in the CG model were determined by fitting the form factor $P(q)$ of mAb2 at 5 mg/mL in 250 mM Arg, as the PPIs were weakest for this system. The short-range attractions between beads i and j of two mAbs are described by a Yukawa pair potential as in Dear et al.:[31]

$$\beta u_{att}\left(\frac{r_{ij}}{d_B}\right) = -\beta K_{ij}\frac{e^{-Z\left(\frac{r_{ij}}{d_B}-1\right)}}{\frac{r_{ij}}{d_B}} \quad (1)$$

where $\beta = (k_BT)^{-1}$, k_B is the Boltzmann constant, T is temperature, and r_{ij}/d_B is the dimensionless interbead separation, with bead diameter $d_B = 3.5$ nm. K_{ij} equals the strength of attraction (K) when both beads i and j are involved in a specific attraction, and zero otherwise, and $Z = 10$ is the dimensionless inverse length scale of attraction which corresponds to a surface to surface separation of ∼0.35 nm. Additionally, a modified Lennard-Jones (LJ) interaction potential adapted from Calero-Rubio et al.[26] is applied between all beads belonging to different mAbs to mimic a uniform vdW background,

$$\beta u_{vdW}\left(\frac{r_{ij}}{d_B}\right) = c\beta\varepsilon_{vdW}\left[\left(\frac{d_B}{r_{ij}}\right)^{128} - \left(\frac{d_B}{r_{ij}}\right)^{6}\right] \quad (2)$$

where $\varepsilon_{vdW} = 0.27k_BT$ is the attraction strength and $c = 1.2196$ is chosen so that the minimum of the LJ-type potential equals $-\varepsilon_{vdW}$. Finally, repulsive electrostatic interaction between two beads is applied using a screened Coulomb potential,[26,27]

$$\beta u_{el}\left(\frac{r_{ij}}{d_B}\right) = \zeta q^2\frac{e^{-\kappa\left(\frac{r_{ij}}{d_B}-1\right)}}{\frac{r_{ij}}{d_B}\left[1 + \frac{1}{2}(\kappa d_B)\right]^2} \quad (3)$$

where $\zeta = (4\pi\varepsilon_0\varepsilon_r k_BT)^{-1}$ is the Bjerrum length with relative permittivity $\varepsilon_r = 78.2$, q is the charge on the bead, and κ is the inverse Debye length calculated from the ionic strength,

$$\kappa = \sqrt{\frac{2N_A I e^2}{k_BT\varepsilon_r}} \quad (4)$$

where N_A is Avogadro's number, I is the ionic strength, and e is the fundamental electron charge. The ionic strength varies from 20 mM (buffer only) to 270 mM for systems with up to 250 mM cosolute corresponding to inverse Debye lengths of ∼2 nm to ∼0.5 nm, respectively. In this work, we fit a single q for all 12 beads to approximate electrostatic repulsion without the need for charge from protein sequence and to minimize the number of adjustable parameters.

The total interaction potential between 2 beads for various representative K, q, and I values is shown in Figure 1A for
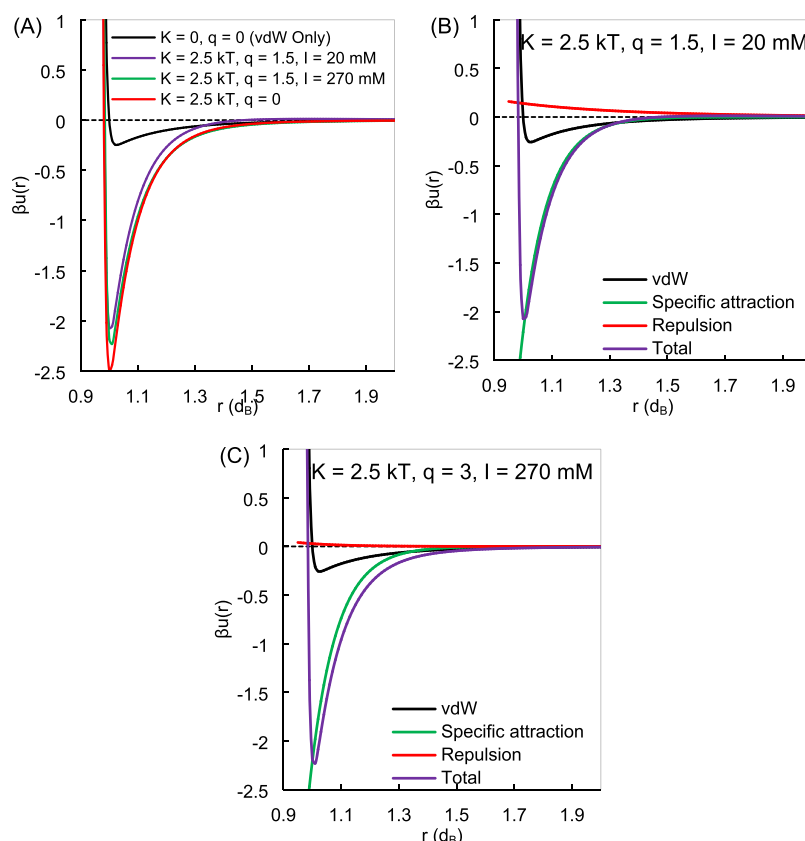
Figure 1. (A) Combined Yukawa (eq 1), 128−6 (eq 2), and screened Coulomb (eq 3) interaction potential between beads i and j as a function of normalized center of mass separation distance for multiple specific attraction strengths, bead charges, and ionic strengths. Contribution of vdW attraction, short-range specific attraction, and electrostatic repulsion on the total interaction potential at (B) low and (C) high ionic strength.

values that will be optimized in the Results and Discussion section. The vdW pair potential is significantly weaker than the short-range bead specific attraction but is present on all 12 beads. The magnitude and length scale of electrostatic repulsion increase with decreasing ionic strength, and thus the well depth of the total potential also decreases. The second osmotic virial coefficient B_{22} for these models, an integrated measure of interprotein attraction strength, was computed as described previously.[31] The B_{22} values reported for a given system were normalized by that of the 12 bead model exhibiting only steric repulsion ($B_{22,St} = 57.4d_B^3$, in agreement with values reported in the literature[25]). MD simulations of N = 6000 identical mAbs were performed using LAMMPS to determine $S(q)$, CSDs, and $g_{COM}(r)$ profiles using methods reported in Dear et al.[31] Briefly, the pair correlation function is obtained from the simulated trajectories by randomly distributing n_s = 10 points within the volume of each bead, then calculating the pair correlations between each of these points. The $I(q)$ is calculated by numerical Fourier transform inversion of the pair correlations, and $S(q)$ is obtained by dividing $I(q)$ at a given concentration by form factor of the 12 bead model. To calculate the CSD, two monomers are considered neighbors if any bead of one is within $r = 1.1d_B$ of the other. Two monomers are considered to be part of the same cluster if they are direct neighbors and/or if they are connected by a continuous path of clustered monomers.

As shown in Table 1, three different models (geometries) of bead-interactions were utilized to probe anisotropic attractions, each including electrostatic repulsion. In all models, the
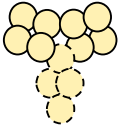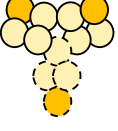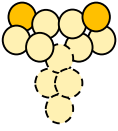
background ε_{vdW} and q on each bead is the same. The vdWR model exhibits no additional bead specific attractions. The All1vdWR model includes short-range attractive potentials between one bead of each Fab domain and the terminal bead of the Fc region to capture Fab−Fab, Fab−Fc, and Fc−Fc ("3-arm") interactions, while the FabFab1vdWR model includes only Fab−Fab ("2-arm") interactions. In this nomenclature the number 1 means one bead in a four bead Fab or Fc section.

■ RESULTS AND DISCUSSION

As shown in Figure 2A for 125 mg/mL mAb2, we obtain a wide range of $S(q)$ PPI behavior upon varying the concentration of NaCl and also by adding Arg at 250 mM. In 30 mM pH 5.5 sodium acetate buffer without NaCl or Arg, the relative net attraction ($S(0) \sim 0.3$) is the weakest and without an inflection at low q ($q < 0.03$ Å^{-1}). With the addition of NaCl up to 250 mM, $S(0)$ increases, indicating greater net attraction. However, as seen in Figure S1, a further increase in NaCl does not increase the net attraction, but instead it decreases above 400 mM. In addition to a change in $S(0)$, the curvature at low q also changes with increasing NaCl, with $S(q)$ flattening out at 50 mM and showing a distinct upward curvature at NaCl concentrations of ≥250 mM. The addition of 250 mM Arg increases $S(0)$ slightly compared to the buffer only control, far less than NaCl at the same ionic strength.

In Figure 2A good fits of $S(q)$ are given for the combination of a uniform vdW and electrostatic repulsion terms, and a tunable specific bead attraction strength K. The $S(q)$ of the

Table 1. Shape and Interaction Geometry of Rigid 12-Bead Models Used for the MD Simulations[a]

12-bead model	specific interaction types	# beads with specific attractions	diagram
vdWR	None	0	
All1vdWR	-Fab-Fab -Fab-Fc -Fc-Fc	3	
FabFab1vdWR	-Fab-Fab	2	

[a]The beads with dashed boundaries represent the Fc region, and beads with solid boundaries represent the Fab regions. (a) Yellow beads interact via the weak 128−6 attraction of eq 2 and the electrostatic repulsion of eq 3. (b) Orange beads interact via the potentials in (a) as well as the stronger short ranged Yukawa attraction of eq 1.

250 mM Arg system is fit using the vdWR model, with $\varepsilon_{vdW} = 0.27k_BT$, $q = 0$, and $K = 0$. Due to the high ionic strength, electrostatic interactions can be neglected.[25,31] In addition, arginine has been shown to inhibit local, short-range interactions both in general[28−36] and for this mAb in particular.[31] Therefore, we use this system to fit ε_{vdW} for all of the other systems where q and K may be nonzero. The All1vdWR model with $K = 2.5k_BT$ and $q = 1.5$ most accurately describes the structure of the 250 mM NaCl system. Furthermore, the same parameters provide accurate approximations for the 50 mM NaCl and buffer only systems, indicating the model is accurate for including the effect of Debye length for the assumed uniform electrostatic repulsion (Figure 1). At high ionic strength, the Debye length is similar to the length scale of attraction and the magnitude and length scale of repulsion are small (Figure 1C). Therefore, the total potential resembles a purely attractive potential with a less attractive well (Figure 1A). As the ionic strength decreases, the increased Debye length results in stronger, more long-range electrostatic repulsion (Figure 1B). The resulting total interaction potential exhibits a weaker attractive well (Figure 1A), leading to a more repulsive $S(q)$, even though K remains unchanged. The calculated effective net protein charge of ~18 at a pH of 5.5 is similar to theoretical values reported previously[14,22,26] at pH away from the pI, suggesting that the net charge can be estimated qualitatively using this method. The goodness of fit to the models exhibiting electrostatic repulsion is quantified using RMSD calculated for $q < 0.06$ Å^{-1} (Table S1), which corresponds to length scales greater than the mAb monomer.

To describe the behavior in real space, the nature of reversible oligomers in these mAb solutions can be characterized by analyzing the $g_{COM}(r)$ (Figure 2B) and CSD
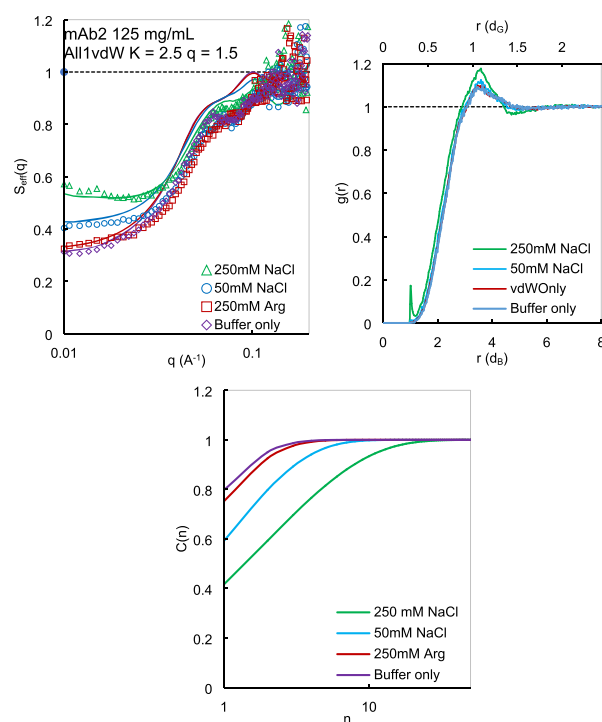
Figure 2. (A, top left) Experimental $S(q)$ profiles of mAb systems (points) along with best fit simulated $S(q)$ for (A) All1vdWR model (solid lines). Experimental $S(q)$ profiles were adapted from Dear et al.[31] (B, top right) Center-of-mass radial distribution functions ($g_{COM}(r)$) for simulations in (A). (C, bottom) Cumulative cluster size distributions for best fit simulations in (A). The values of K and q are indicated for all systems except 250 mM Arg where they are both zero.

(Figure 2C) profiles of the simulations that best fit the $S(q)$ profile. For the buffer only and the vdWR system that best fits the 250 mM Arg solution, the $g_{COM}(r)$ profile indicates relatively weak interactions with a small peak and lack of longer ranged structure. Here approximately 80% of the mAb is in the monomer form as shown by the CSD in Figure 2C (magenta lines). For the simulation that matches $S(q)$ of the 50 mM NaCl system, the magnitude of the peak corresponding to twice the radius of gyration of the entire 12 bead model, $d_G \sim$ 10 nm, (r $\sim 1.1d_G$) increases relative to the vdWR system. A center of mass (COM) separation of $\sim 1d_G$ corresponds to interactions between terminal beads on the model, so the increase in the peak height suggests more particles interacting via the stronger specific bead attraction sites, resulting in greater self-association. Here, monomer amount is approximately 60% with the rest mostly dimers and trimers. At the highest ionic strength, where repulsion is screened (green lines, best fit to 250 mM NaCl data), there is a larger dip in $g_{COM}(r)$ below unity at r $\sim 1.4d_G$ relative to the vdWR model and a slight peak at r $\sim 2d_G$, indicating oscillations beyond the first coordinate shell that are associated with greater self-association. The $g_{COM}(r)$ also increases at r $< 1d_G$, suggesting interactions between domains of two particles (Fab or Fc domains) which are possible because the vdW attraction on each bead allows multibead interactions to be energetically favorable to overcome the entropic penalty of such configurationally restrictive interactions. As can be seen in the CSD, monomers now account for only 40% of the solution and oligomers of over 10 monomers are present.
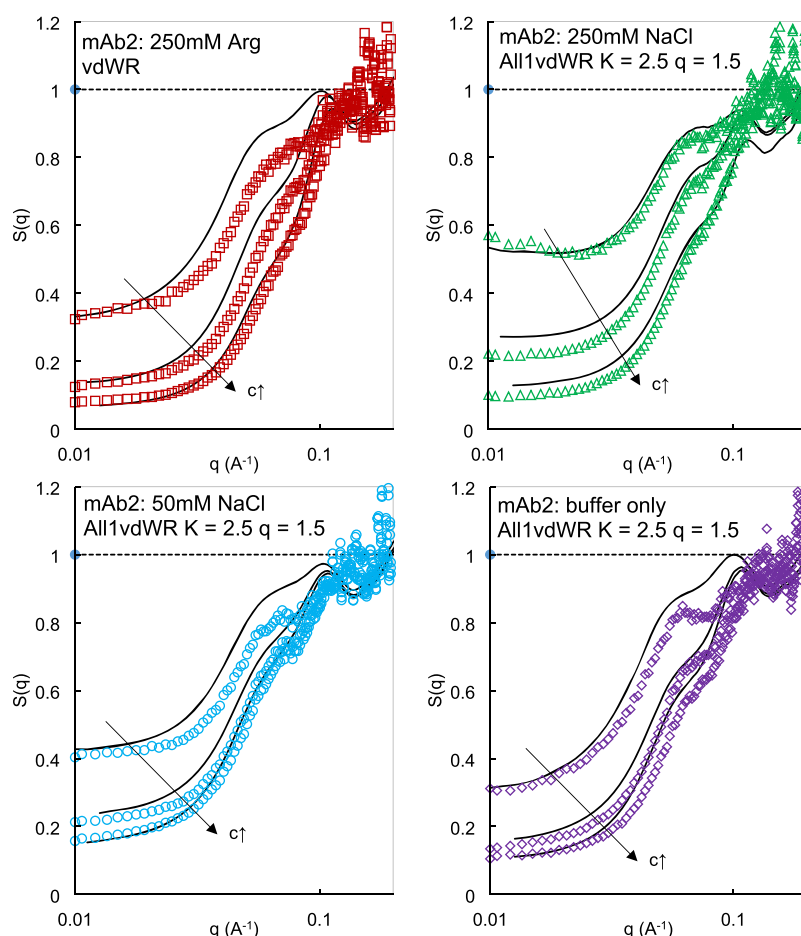
Figure 3. $S(q)$ profiles (points) for different mAb2 systems at 125, 200, and 250 mg/mL with simulated $S(q)$ profiles (lines) for the different models at the same concentrations using K and q obtained from fitting data at 125 mg/mL.

To evaluate the effect of electrostatic repulsion on $S(q)$, the same set of experimental data were fit with a force field that excluded the screened Coulomb potential (All1vdW model), shown in Figure S2A. While the All1vdW model provides good fits to the data, the strength of anisotropic attraction (K) had to be fit separately for each curve to account for the change in PPI due to ionic strength, as in our earlier work.[31,32] Furthermore, even at high ionic strength some electrostatic repulsion is still present. Thus, the best fit K is lower than the true value, as it compensates indirectly for the residual electrostatic repulsion. Therefore, the inclusion of uniform electrostatic repulsion is highly advantageous in that K and q were constant while varying the ionic strength over a wide range with NaCl.

In Figure 3, we predict the effect of protein concentration for the four key systems. The models with attraction strength (K) tuned at an intermediate mAb concentration of 125 mg/mL provide good predictions $S(q)$ profiles at concentrations up to 250 mg/mL for all systems tested without any changes in the ε_{vdW}, K, and q. As the protein concentration increases, the $S(q)$ becomes more repulsive in all cases because of excluded volume effects. Consequently, it becomes harder to distinguish the effect of cosolute on the PPI at concentrations greater than 200 mg/mL as the discrimination between $S(q)$ curves diminishes. However, the ability of our model to predict the change in experimental $S(q)$ curves with protein concentration without any variation in parameters suggests that the model is

accurate for these conditions. Thus, since K and q remain constant across concentration, the differences in the $S(q)$ profiles are due primarily to steric repulsion from closer mAb proximity rather than a change in the intermolecular potentials. In the future, it would be of interest to study lower protein concentrations from 5 to 100 mg/mL to further study this behavior, as done previously for a polyclonal antibody.[32]

The importance of including electrostatic repulsion, especially at low ionic strength, becomes more evident when extrapolating fits to higher protein concentrations. Figure S3 shows the same experimental data approximated using models that do not include electrostatic repulsion, with K tuned at the same concentration of 125 mg/mL. At high ionic strength, the fits using the All1vdW model (Figure S3A and S3B) are comparable to those using the All1vdWR model with electrostatic repulsion. However, at low ionic strength for 0 or 50 mM NaCl, the prediction of All1vdW model tuned at 125 mg/mL is more repulsive than the experimental data at 200 and 250 mg/mL (Figure S3C and S3D). As discussed above, fitting experimental data with a model that does not include electrostatic repulsion results in values of the short-range anisotropic attraction that are unphysically small as they compensate for the missing electrostatic repulsion. Thus, the model does not predict enough attraction as the concentration increases and the $S(q)$ values are too small. Thus, the ability of the new model with explicit electrostatic repulsion to predict
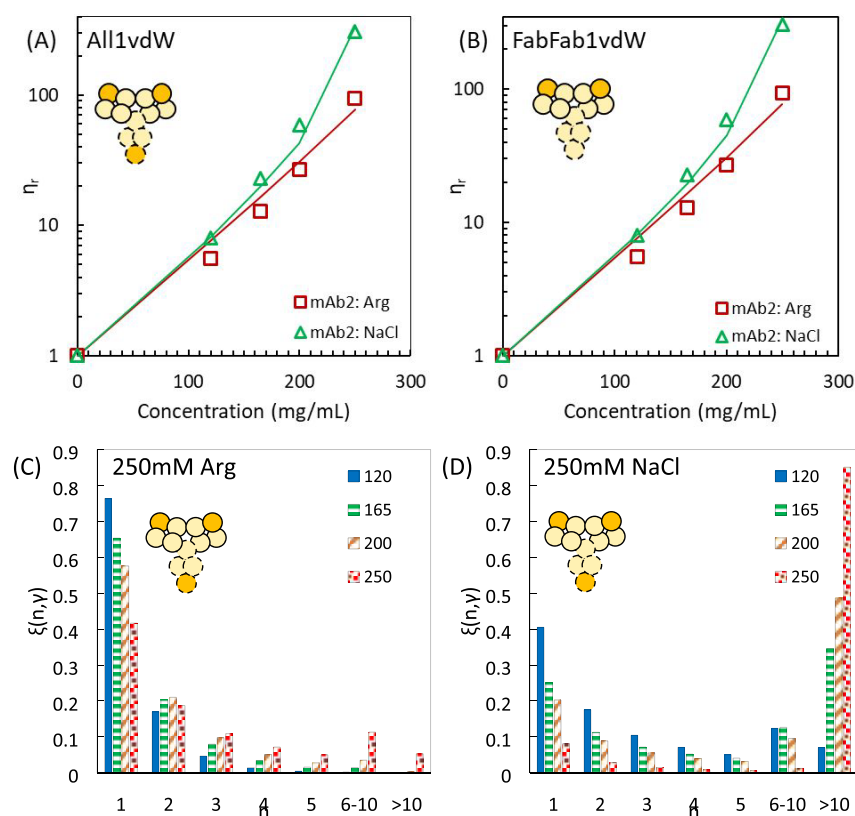
Figure 4. (Top) Measured relative viscosity vs mAb concentration for mAb2:Arg and mAb2:NaCl with corresponding fits to eq 5 (lines) using CSD from (A) best-fit All1vdW systems and (B) best fit FabFab1vdW systems. (Bottom) Histograms of relative contribution of n-mers to viscosity using CSD of best fit All1vdW system for (C) mAb2:Arg and (D) mAb2:NaCl.

the change in $S(q)$ with protein concentration (Figure 3) is highly advantageous.

We now examine the effect of adding uniform vdW attraction to bead specific attraction for models that do not include electrostatic repulsion. To do this, we compare new simulations with very recent models that only included specific bead attraction without a vdW background[31] (Figure S4) (these models were named All4, All1, and FabFab1). In the uniform All4 model, every bead exhibits only a short ranged attraction based on eq 1. The All1 and FabFab1 models contain short ranged attraction (eq 1) in the same geometry as the corresponding vdW models but do not include the uniform vdW attraction or electrostatic repulsion. The unphysical peak at $q \sim 0.06$ A^{-1} and trough at $q \sim 0.1$ A^{-1} (Figure S4A and S4B) in the All1 model are removed with the inclusion of the uniform vdW attraction in the All1vdW model. The two new All1vdW and FabFab1vdW models that best fit the 50 mM NaCl system do not exhibit the sharp unphysical peak previously seen in the $g_{COM}(r)$ of the previous All4 model that did not include the vdW background (Figure S4C and S4D). Furthermore, the degree of clustering with the new models is reduced compared to the previous All1 and FabFab1 models (Figure S4E and S4F) given the smaller difference in attraction strength on the specifically interacting beads relative to the other beads. This smaller difference is also evident in the lower K values on beads with specific attraction in the new models. Further discussion on the differences between the two classes of models can be found in the Supporting Information.

It is instructive to contrast $S(q)$ and the real space properties $g_{COM}(r)$ and CSD for two (FabFab1vdW) and three arm

(All1vdW) models for the same overall attraction strength as quantified by $B_{22}/B_{22,St}$ (Figure S5). Whereas this comparison of effect of the location of bead specific interaction is performed without including electrostatic repulsion, similar results would be obtained if they are included. For weakly attractive systems with $B_{22}/B_{22,St}$ values of 0.70 and 0.60, $S(q)$ and $g_{COM}(r)$ profiles are nearly identical for the All1vdW and FabFab1vdW models despite higher required K values for the FabFab1vdW (Figure S5A and S5B). The CSDs for $B_{22}/B_{22,St}$ = 0.70 are also similar; however, for $B_{22}/B_{22,St}$ = 0.60, the CSD for the FabFab1vdW model, which has a larger specific bead attraction strength, shows a greater degree of self-association (Figure S5C). Here, the attraction is concentrated on a smaller number of beads. For more attractive systems with $B_{22}/B_{22,St} <$ 0.40, the $S(q)$, $g_{COM}(r)$, and CSD of the two models become qualitatively far more different. For FabFab1vdW, the upturn begins at $q \sim 0.04$ A^{-1} and levels off at $q \sim 0.01$ A^{-1}, whereas for All1vdW the upturn begins at a lower $q \sim 0.03$ A^{-1} and does not level off within the q range measured. Significantly larger clusters in CSD are observed for the FabFab1vdW system given the high K value. Notice that the CSD is sensitive to the magnitude of the bead specific attraction strength when B_{22} is constant, highlighting the importance of including anisotropy in attraction when predicting clustering and viscosities.

The viscosities of the different mAb systems versus concentration are fit using an adaptation[31,32] of the model developed by Kastelic et al.[33] to account for the degree of clustering in solution:

$$\ln(\eta_r) = \sum_{n=1}^{\infty} \gamma\, f(n)\, p(n,\gamma)$$

$$f(n) = bn^d \tag{5}$$

where η_r is the relative viscosity, γ the mass concentration of protein, b and d are adjustable parameters, and $p(n,\gamma)$ is the normalized, mass fraction distribution of clusters of size n, as represented by the CSD from the best fit simulations of $S(q)$. Only one set of b and d are used to fit all the curves. Figure 4A and Figure 4B show the fits of eq 5 to experimental viscosity for the CSD for the All1vdW and FabFab1vdW models (which do not include electrostatic repulsion), respectively. (Similar results, not shown, are obtained with the All1vdWR versus All1vdW models, since the CSDs were very similar as shown in Figures 2 and S6.) As shown in Figure 4A and Figure 4B, the Kastelic model accurately represents the viscosities of 250 mM Arg and 250 mM NaCl systems at high concentrations equally well based on CSDs from the 3- and 2-arm models. Even for the 250 mM NaCl case, the lack of distinction is due to the similar CSDs of the two models across protein concentrations (Figure S6). Finally, to demonstrate that lower and higher viscosity systems stem from very different distributions of oligomer sizes, the fractional contribution of n-mers on viscosity, $\xi(n,\gamma)$ (eq 6), is calculated based on the definition in Kastelic et al.[33]

$$\xi = \frac{f(n)\, p(n,\gamma)}{\sum_{n=1}^{\infty} f(n)\, p(n,\gamma)} \tag{6}$$

As shown in Figure 4C, for 250 mM Arg, the viscosity is influenced primarily by monomers, with the impact of small oligomers increasing with mAb concentration, and oligomers with $n > 10$ only playing a role at 250 mg/mL. In contrast, the viscosity for 250 mM NaCl is determined more by the small oligomeric species even at 125 mg/mL, and the effect of larger oligomers increases with concentration (Figure 4D), where much larger clusters with $n > 10$ become dominant (Figure S6D) by 250 mg/mL and corresponding viscosities exceed 200 cP. At concentrations close to maximum packing, viscosity is affected by a complex set of factors, such as the molecule shape, strength of interactions, and length scale of interactions, some of which may not be adequately described by our model. For example, the flexibility of the hinge region may affect the equilibrium shape adopted by the mAb as well as the structure of packing, especially at high concentrations, which is not captured by our rigid models. Additionally, we assume that the parameters in the applied force field (strength and length scale of interaction) remain constant across concentration, but this may not be true at high concentrations when surface interactions are affected by the close proximity of other molecules. However, the bead specific model concept may be adapted in future studies to relax these simplifying assumptions.

CONCLUSIONS

The PPI and self-association of a mAb in response to protein concentration, ionic strength, and cosolutes are characterized by interpreting experimental SAXS $S(q)$ profiles with MD simulations. A systematic method is presented to regress three parameters to describe uniform electrostatic repulsion and vdW attraction on each bead as well as anisotropic short-range bead-specific attraction. The best fits of SAXS $S(q)$ data with

simulation provide the strength of short-range attraction with the ability to discriminate between attraction in various locations (e.g., Fab−Fab vs Fab−Fab and Fab−Fc interactions). Furthermore, upon including electrostatic repulsion (with uniform bead charge q) and uniform vdW attraction on each bead, $S(q)$ may be predicted for protein concentrations from 125−250 mg/mL and ionic strengths from 20−270 mM with a single constant parameter (K) to describe anisotropic short-range attraction. With the inclusion of the uniform vdW attraction, the $S(q)$ fits become much more accurate at q values above 0.06 Å^{-1} at intermediate length scales, given less variation in attraction strength among beads. The good fits of the experimental SAXS $S(q)$ over a wide q range provide a rationale for determining radial distribution functions and cluster size distributions to better understand protein structure in solution. The CSDs shed novel insight into the nature of self-association and its influence on viscosity and ultimately on protein stability. The rapid advances in experimental SAXS data along with CG MD simulations to interpret the protein interactions and structure at high concentration may be expected to be highly complementary to more established techniques such as static light scattering that only cover very low q values to potentially guide mAb, discovery, processing, and formulation.

■ ASSOCIATED CONTENT

Ⓢ Supporting Information

The Supporting Information is available free of charge at https://pubs.acs.org/doi/10.1021/acs.molpharmaceut.9b00960.

> Comparisons of the vdW model with models previously published; $S(q)$ at multiple ionic strengths; RMSD fits of simulated $S(q)$ to experimental data; fits to experimental data using models that do not include electrostatic repulsion; comparison of simulations at the same B_{22}; CSD for systems at additional concentrations (PDF)

■ AUTHOR INFORMATION

Corresponding Authors

Keith P. Johnston − *McKetta Department of Chemical Engineering, The University of Texas at Austin, Austin, Texas 78712, United States; Center for Integrated Nanotechnologies, Sandia National Laboratories, Albuquerque, New Mexico 87185, United States;* ⓞ orcid.org/0000-0002-0915-1337; Phone: 512 471 4617; Email: kpj@che.utexas.edu; Fax: 512 471 7060

Thomas M. Truskett − *McKetta Department of Chemical Engineering and Department of Physics, The University of Texas at Austin, Austin, Texas 78712, United States;* ⓞ orcid.org/0000-0002-6607-6468; Email: truskett@che.utexas.edu

Authors

Amjad Chowdhury − *McKetta Department of Chemical Engineering and Texas Materials Institute, The University of Texas at Austin, Austin, Texas 78712, United States;* ⓞ orcid.org/0000-0003-3226-4310

Jonathan A. Bollinger − *Center for Integrated Nanotechnologies, Sandia National Laboratories, Albuquerque, New Mexico 87185, United States*

Barton J. Dear − *McKetta Department of Chemical Engineering and Texas Materials Institute, The University of Texas at Austin, Austin, Texas 78712, United States*

Jason K. Cheung — *Pharmaceutical Sciences, MRL, Merck & Co., Inc., Rahway, New Jersey 07065, United States*

■ ACKNOWLEDGMENTS

■ REFERENCES

(1) Antibody Society. Antibody therapeutics approved or in regulatory review in the EU or US. https://www.antibodysociety.org/resources/%20approved-antibodies/. (accessed 2019-12-04).

(2) Yadav, S.; Laue, T. M.; Kalonia, D. S.; Singh, S. N.; Shire, S. J. The influence of charge distribution on self-association and viscosity behavior of monoclonal antibody solutions. *Mol. Pharmaceutics* **2012**, *9* (4), 791−802.

(3) Quang, L. J.; Sandler, S. I.; Lenhoff, A. M. Anisotropic contributions to protein-protein interactions. *J. Chem. Theory Comput.* **2014**, *10* (2), 835−845.

(4) Laue, T. Proximity energies: a framework for understanding concentrated solutions. *J. Mol. Recognit.* **2012**, *25* (3), 165−173.

(5) Chari, R.; Jerath, K.; Badkar, A. V.; Kalonia, D. S. Long-and short-range electrostatic interactions affect the rheology of highly concentrated antibody solutions. *Pharm. Res.* **2009**, *26* (12), 2607−2618.

(6) Shire, S. J.; Shahrokh, Z.; Liu, J. Challenges in the development of high protein concentration formulations. *J. Pharm. Sci.* **2004**, *93* (6), 1390−1402.

(7) Roberts, C. J. Protein aggregation and its impact on product quality. *Curr. Opin. Biotechnol.* **2014**, *30*, 211−217.

(8) Connolly, B. D.; Petry, C.; Yadav, S.; Demeule, B.; Ciaccio, N.; Moore, J M. R.; Shire, S. J.; Gokarn, Y. R. Weak Interactions Govern the Viscosity of Concentrated Antibody Solutions: High-Throughput Analysis Using the Diffusion Interaction Parameter. *Biophys. J.* **2012**, *103* (1), 69−78.

(9) Dear, B. J.; Hung, J. J.; Truskett, T. M.; Johnston, K. P. Contrasting the Influence of Cationic Amino Acids on the Viscosity and Stability of a Highly Concentrated Monoclonal Antibody. *Pharm. Res.* **2017**, *34* (1), 193−207.

(10) Yadav, S.; Shire, S. J.; Kalonia, D. S. Factors Affecting the Viscosity in High Concentration Solutions of Different Monoclonal Antibodies. *J. Pharm. Sci.* **2010**, *99* (12), 4812−4829.

(11) Yadav, S.; Shire, S. J.; Kalonia, D. S. Viscosity Behavior of High-concentration Monoclonal Antibody Solutions: Correlation with Interaction Parameter and Electroviscous Effects. *J. Pharm. Sci.* **2012**, *101* (3), 998−1011.

(12) Saito, S.; Hasegawa, J.; Kobayashi, N.; Kishi, N.; Uchiyama, S.; Fukui, K. Behavior of monoclonal antibodies: relation between the second virial coefficient (B (2)) at low concentrations and aggregation propensity and viscosity at high concentrations. *Pharm. Res.* **2012**, *29* (2), 397−410.

(13) Ghosh, R.; Calero-Rubio, C.; Saluja, A.; Roberts, C. J. Relating protein-protein interactions and aggregation rates from low to high concentrations. *J. Pharm. Sci.* **2016**, *105* (3), 1086−1096.

(14) Yearley, E. J.; Zarraga, I. E.; Shire, S. J.; Scherer, T. M.; Gokarn, Y.; Wagner, N. J.; Liu, Y. Small-angle neutron scattering characterization of monoclonal antibody conformations and interactions at high concentrations. *Biophys. J.* **2013**, *105* (3), 720−731.

(15) Fukuda, M.; Moriyama, C.; Yamazaki, T.; Imaeda, Y.; Koga, A. Quantitative correlation between viscosity of concentrated mAb solutions and particle size parameters obtained from small-angle x-ray scattering. *Pharm. Res.* **2015**, *32* (12), 3803−3812.

(16) Fukuda, M.; Watanabe, A.; Hayasaka, A.; Muraoka, M.; Hori, Y.; Yamazaki, T.; Imaeda, Y.; Koga, A. Small-scale Screening Method for Low-viscosity Antibody Solutions Using Small-angle X-ray Scattering. *Eur. J. Pharm. Biopharm.* **2017**, *112*, 132−137.

(17) Wang, W.; Lilyestrom, W. G.; Hu, Z. Y.; Scherer, T. M. Cluster size and quinary structure determine the rheological effects of antibody self-association at high concentrations. *J. Phys. Chem. B* **2018**, *122* (7), 2138−2154.

(18) Scherer, T. M.; Liu, J.; Shire, S. J.; Minton, A. I. Intermolecular interactions of IgG1 monoclonal antibodies at high concentrations characterized by light scattering. *J. Phys. Chem. B* **2010**, *114* (40), 12948−12957.

(19) Lilyestrom, W. G.; Yadav, S.; Shire, S. J.; Scherer, T. M. Monoclonal antibody self-association, cluster formation, and rheology at high concentrations. *J. Phys. Chem. B* **2013**, *117* (21), 6373−6384.

(20) Scherer, T. M. Role of Cosolute-Protein Interactions in the Dissociation of Monoclonal Antibody Clusters. *J. Phys. Chem. B* **2015**, *119* (41), 13027−13038.

(21) Hung, J. J.; Dear, B. J.; Karouta, C. A.; Chowdhury, A. A.; Godfrin, P. D.; Bollinger, J. A.; Nieto, M. P.; Wilks, L. R.; Shay, T. Y.; Ramachandran, K.; Sharma, A.; Cheung, J. K.; Truskett, T. M.; Johnston, K. P. Protein-Protein Interactions of Highly Concentrated Monoclonal Antibody Solutions via Static Light Scattering and Influence on the Viscosity. *J. Phys. Chem. B* **2019**, *123* (4), 739−755.

(22) Chaudhri, A.; Zarraga, I. E.; Kamerzell, T. J.; Brandt, J. P.; Patapoff, T. W.; Shire, S. J.; Voth, G. A. Coarse-grained modeling of the self-association of therapeutic monoclonal antibodies. *J. Phys. Chem. B* **2012**, *116* (28), 8045−8057.

(23) Buck, P. M.; Chaudhri, A.; Kumar, S.; Singh, S. K. Highly viscous antibody solutions are a consequence of network formation caused by domain-domain electrostatic complementarities: insights from coarse-grained simulations. *Mol. Pharmaceutics* **2015**, *12* (1), 127−139.

(24) Chaudhri, A.; Zarraga, I. E.; Yadav, S.; Patapoff, T. W.; Shire, S. J.; Voth, G. A. The role of amino acid sequence in the self-association of therapeutic monoclonal antibodies: insights from coarse-grained modeling. *J. Phys. Chem. B* **2013**, *117* (5), 1269−1279.

(25) Calero-Rubio, C.; Saluja, A.; Roberts, C. J. Coarse-grained antibody models for "weak" protein-protein interactions from low to high concentrations. *J. Phys. Chem. B* **2016**, *120* (27), 6592−6605.

(26) Calero-Rubio, C.; Ghosh, R.; Saluja, A.; Roberts, C. J. Predicting protein-protein interactions of concentrated antibody solutions using dilute solution data and coarse-grained molecular models. *J. Pharm. Sci.* **2018**, *107* (5), 1269−1281.

(27) Wang, G.; Varga, Z.; Hofmann, J.; Zarraga, I. E.; Swan, J. W. Structure and relaxation in solutions of monoclonal antibodies. *J. Phys. Chem. B* **2018**, *122* (11), 2867−2880.

(28) Barnett, G. V.; Razinkov, V. I.; Kerwin, B. A.; Hillsley, A.; Roberts, C. J. Acetate- and Citrate-Specific Ion Effects on Unfolding and Temperature-Dependent Aggregation Rates of Anti-Streptavidin IgG1. *J. Pharm. Sci.* **2016**, *105*, 1066−1073.

(29) Barnett, G. V.; Razinkov, V. I.; Kerwin, B. A.; Blake, S.; Qi, W.; Curtis, R. A.; Roberts, C. J. Osmolyte Effects on Monoclonal Antibody Stability and Concentration-Dependent Protein Interactions with Water and Common Osmolytes. *J. Phys. Chem. B* **2016**, *120*, 3318−3330.

(30) Roberts, D.; Keeling, R.; Tracka, M.; van der Walle, C. F.; Uddin, S.; Warwicker, J.; Curtis, R. Specific Ion and Buffer Effects on Protein-Protein Interactions of a Monoclonal Antibody. *Mol. Pharmaceutics* **2015**, *12* (1), 179−193.

(31) Dear, B. J.; Bollinger, J. A.; Chowdhury, A.; Hung, J. J.; Wilks, L. R.; Karouta, C. A.; Ramachandran, K.; Shay, T. Y.; Nieto, M. P.; Sharma, A.; Godfrin, P. D.; Truskett, T. M.; Johnston, K. P. X-ray Scattering and Coarse-Grained Simulations for Clustering and Interactions of Monoclonal Antibodies at High Concentrations. *J. Phys. Chem. B* **2019**, *123*, 5274−5290.

(32) Chowdhury, A.; Guruprasad, G.; Chen, A. T.; Karouta, C. A.; Blanco, M. A.; Truskett, T. M.; Johnston, K. P. Protein-protein interactions, clustering, and rheology for bovine IgG up to high concentrations characterized by small angle x-ray scattering and molecular dynamics simulations. *J. Pharm. Sci.* **2020**, *109*, 696−708.

(33) Kastelic, M.; Dill, K. A.; Kalyuzhnyi, Y. V.; Vlachy, V. Controlling the viscosities of antibody solutions through control of their binding sites. *J. Mol. Liq.* **2018**, *270*, 234−242.

(34) Arakawa, T.; Ejima, D.; Tsumoto, K.; Obeyama, N.; Tanaka, Y.; Kita, Y.; Timasheff, S. N. Suppression of protein interactions by arginine: a proposed mechanism of the arginine effects. *Biophys. Chem.* **2007**, *127* (1), 1−8.

(35) Shukla, D.; Trout, B. L. Interaction of arginine with proteins and the mechanism by which it inhibits aggregation. *J. Phys. Chem. B* **2010**, *114* (42), 13426−13438.

(36) Shukla, D.; Trout, B. L. Preferential Interaction Coefficients of Proteins in Aqueous Arginine Solutions and Their Molecular Origins. *J. Phys. Chem. B* **2011**, *115* (5), 1243−1253.

(37) Blanco, M. A.; Sahin, E.; Robinson, A. S.; Roberts, C. J. Coarse-Grained Model for Colloidal Protein Interactions, B-22, and Protein Cluster Formation. *J. Phys. Chem. B* **2013**, *117* (50), 16013−16028.